

Gravitational Waves as a Probe of Globular Cluster Formation and Evolution

Isobel M. Romero-Shaw,^{1,2*} Kyle Kremer,^{3,4} Paul D. Lasky,^{1,2} Eric Thrane^{1,2} and Johan Samsing⁵

¹Monash Centre for Astrophysics, School of Physics and Astronomy, Monash University, VIC 3800, Australia

²OzGrav: The ARC Centre of Excellence for Gravitational-wave Discovery, Clayton, VIC 3800, Australia

³TAPIR, California Institute of Technology, Pasadena, CA 91125, USA

⁴The Observatories of the Carnegie Institution for Science, Pasadena, CA 91101, USA

⁵Niels Bohr International Academy, The Niels Bohr Institute, Blegdamsvej 17, 2100 Copenhagen, Denmark

Accepted XXX. Received YYY; in original form ZZZ

ABSTRACT

Globular clusters are considered to be likely breeding grounds for compact binary mergers. In this paper, we demonstrate how the gravitational-wave signals produced by compact object mergers can act as tracers of globular cluster formation and evolution. Globular cluster formation is a long-standing mystery in astrophysics, with multiple competing theories describing when and how globular clusters formed. The limited sensitivity of electromagnetic telescopes inhibits our ability to directly observe globular cluster formation. However, with future audio-band detectors sensitive out to redshifts of $z \approx 50$ for GW150914-like signals, gravitational-wave astronomy will enable us to probe the Universe when the first globular clusters formed. We simulate a population of binary black hole mergers from theoretically-motivated globular cluster formation models, and construct redshift measurements consistent with the predicted accuracy of third-generation detectors. We show that we can locate the peak time of a cluster formation epoch during reionisation to within 0.05 Gyr after one year of observations. The peak of a formation epoch that coincides with the Universal star formation rate can be measured to within 0.4 Gyr—10.5 Gyr after one year of observations, depending on the relative weighting of the model components.

Key words: globular clusters: general – galaxies: star formation – dark ages, reionization, first stars – stars: black holes – gravitational waves

1 INTRODUCTION

The first detections of gravitational waves, made over the last five years (Abbott et al. 2019; Abbott et al. 2020c), provide a new lens through which to observe the Universe. Advanced LIGO (Aasi et al. 2015) and Virgo (Acernese et al. 2015) have confirmed the existence of multiple phenomena that, prior to the era of gravitational-wave astronomy, had only been theoretically proposed; stellar-mass binary black holes (BBH) (Abbott et al. 2016), merging neutron stars (Abbott et al. 2017b,c), and intermediate-mass black holes (Abbott et al. 2020b) have all been directly observed with gravitational waves.

We are accruing gravitational-wave observations of merging black holes at an accelerating rate (Abbott et al. 2016; Abbott et al. 2019; Abbott et al. 2020c,d). This abundance of BBH merger detections presents a variety of puzzles across theoretical astrophysics. One such question is how BBH systems that merge within the age of the Universe are assembled. If the binary evolves in isolation, this outcome may be achieved via the common envelope process (see, e.g., Livio & Soker 1988; Bethe & Brown 1998; Ivanova et al. 2013; Kruckow et al. 2016), stable mass transfer of a stellar secondary onto the primary black hole (van den Heuvel et al. 2017; Neijssel

et al. 2019; Bavera et al. 2021), chemically homogeneous evolution (de Mink et al. 2010; de Mink & Mandel 2016) and/or ambient gas-driven fallback (Tagawa et al. 2018). Alternatively, the compact object binary may form dynamically. In this case, the two components evolve separately, only encountering one another once they are already black holes. For this encounter to take place, the components must reside in an environment facilitating dynamical interactions. Such environments include active galactic nuclei (e.g., Gröbner et al. 2020), nuclear star clusters (e.g., Hoang et al. 2018; Fragione & Kocsis 2018), young massive clusters (Di Carlo et al. 2019) and globular clusters (e.g., Rodriguez et al. 2015; Hong et al. 2018). In globular clusters, mass segregation leads to the formation of a dark compact-object core (see, e.g., Morscher et al. 2015; Wang et al. 2016; Kremer et al. 2020a), where black holes may interact and merge dynamically. Evidence from LIGO–Virgo’s third observing run suggests that a substantial fraction ($\approx 25 - 93\%$ with 90% credibility) of merging BBH form dynamically (Abbott et al. 2020d); see also Abbott et al. (2020b); Abbott et al. (2020a); Romero-Shaw et al. (2020b); Zevin et al. (2020).

The gravitational-wave signal from a binary compact object merger carries information about the source’s component masses, component spins, and orbital eccentricity. These parameters can be used to distinguish which formation channel the binary evolved through. When a BBH system evolves in isolation, it is expected

* isobel.romero-shaw@monash.edu

to have component masses $m \lesssim 65 M_{\odot}$ due to the effects of pair-instability supernovae (e.g., [Heger & Woosley \(2002\)](#); [Fishbach & Holz \(2017\)](#); [Talbot & Thrane \(2018\)](#); see [Belczynski \(2020\)](#) for a review of recent updates to this limit for various stellar populations). The co-evolution of the binary is thought to lead to component spins that are preferentially aligned with the orbital angular momentum ([Kalogera 2000](#); [Campanelli et al. 2006](#); [Stevenson et al. 2017](#); [Talbot & Thrane 2017](#)), and since compact binary orbits circularise through gravitational radiation at a faster rate than their separation reduces, any orbital eccentricity induced by the supernovae of the components becomes negligible by the time the gravitational-wave signal enters the observing band ([Peters 1964](#); [Hinder et al. 2008](#)).¹ When a BBH system forms and merges dynamically, its properties can be detectably different from those of isolated mergers. In the dense environments that support dynamical formation, repeated BH or stellar mergers can give rise to binaries in which one or both components have masses within the pulsational pair-instability mass gap (e.g., [Gerosa & Berti 2017](#); [Samsing & Hotokezaka 2020](#); [Kremer et al. 2020b](#); [Kimball et al. 2020b](#)). Because the components do not co-evolve, their spins may have any orientation relative to each other ([Rodriguez et al. 2016b](#)), and few-body interactions and/or gravitational-wave captures can give rise to mergers with non-negligible eccentricity close to merger (see, e.g., [Samsing et al. 2014](#); [Rodriguez et al. 2018c](#); [Gondán & Kocsis 2019](#); [Samsing et al. 2018](#); [Zevin et al. 2019](#); [Kremer et al. 2020a](#)). In globular clusters, $\sim 5\%$ of all BBH mergers are expected to have significant eccentricity close to merger ($e \geq 0.1$ at 10 Hz) ([Samsing 2018](#); [Samsing & D’Orazio 2018](#); [Rodriguez et al. 2018a,c](#)).

Globular clusters are observed in great quantities, both inside our Galaxy and beyond; there are ≈ 160 known globular clusters in the Milky Way ([SEDS Messier Database 2020](#)), ≈ 500 in the neighbouring Andromeda Galaxy ([Peacock et al. 2010](#)), and ~ 12000 in supergiant elliptical galaxies like M87 ([Tamura et al. 2006](#)). Despite their prolific nature, it is not known how globular clusters form. Globular clusters contain stars that are thought to be among some of the most ancient in their host galaxy (for example, the globular cluster Hpl contains some of the most ancient stars ($\gtrsim 12$ Gyr) in the Milky Way; [Kerber et al. 2019](#)), making their formation difficult to observe with electromagnetic telescopes. To date, the primary method to constrain cluster ages is main-sequence fitting of colour-magnitude diagrams (e.g., [Gratton et al. 1997](#); [Sarajedini et al. 2007](#); [VandenBerg et al. 2013](#)) with a small subset of cluster ages also determined from the white dwarf cooling sequence (e.g., [Hansen et al. 2013](#); [García-Berro et al. 2014](#)). Typical globular cluster age measurements have uncertainties of order $O(1)$ Gyr; see [Forbes et al. \(2015, 2018\)](#) and references therein. It is hoped that the James Webb Space Telescope (JWST)—due to be launched in October, 2021 ([NASA 2020](#))—will be able to constrain cluster ages to within 1 Gyr (e.g., [Correnti et al. 2016](#)).

Measurements of globular cluster ages and metallicities suggest two different globular cluster sub-populations: very old globular clusters, which are observed to have a wide range of ages and metallicities; and younger globular clusters, which have metallicities that anticorrelate with their ages ([Hansen et al. 2013](#); [Forbes & Bridges 2010](#); [VandenBerg et al. 2013](#); [Leaman et al. 2013](#); [Forbes et al. 2015](#)). Current theories of globular cluster formation fall into two main cat-

egories: (i) clusters formed as a byproduct of active star formation in galaxy discs (e.g., [Elmegreen 2010](#); [Shapiro et al. 2010](#); [Kruijssen 2015](#)) and (ii) clusters formed due to the collapse of dark matter halos during or before the epoch of reionisation (e.g., [Fall & Rees 1985](#); [Katz & Ricotti 2014](#); [Ramirez-Ruiz et al. 2015](#); [Trenti et al. 2015](#); [Kimm et al. 2016](#); [Ma et al. 2020](#)). In category (i), the formation probability follows the observed star formation rate (SFR; [Madau & Dickinson 2014](#)), peaking at $z \approx 2.5$ ([Forbes et al. 2015, 2018](#)), while in category (ii) the formation probability peaks at $6 \lesssim z \lesssim 12$ ([Forbes et al. 2015](#); [Trenti et al. 2015](#)).

Constraining the primary formation epoch of globular clusters will answer long-established questions in astrophysics. If globular clusters predominantly form before $z \approx 6$, they may play a leading role in the reionisation of the Universe (e.g., [Ma et al. 2020](#)). On the other hand, if the globular cluster formation probability curve follows the SFR, and the majority of star formation takes place in such environments (e.g., [Lada & Lada 2003](#)), then detailed understanding of cluster formation histories may place critical constraints upon the overall SFR. If we know the formation epoch of clusters, then we can adjust N-body simulations to more correctly reproduce clusters observed at $z = 0$, thereby enhancing our physical descriptions of cluster initial conditions. Our understanding of the role that globular clusters play in the evolution of galaxies—for example, whether globular clusters are early galaxies ([Elmegreen & Elmegreen 2017](#)), failed galaxies ([Fall & Rees 1985](#)), or galaxy remnants ([Majewski et al. 2000](#))—can also be improved by observing globular clusters as they form and evolve.

As detectors improve, gravitational waves will allow us to trace compact binary mergers throughout cosmic time (see, e.g., [Vitale et al. 2019](#); [Safarzadeh et al. 2019](#)). In turn, this will allow us to use gravitational waves as probes of cluster formation and evolution. The current generation of detectors can observe events out to redshifts $z \lesssim 1.5$ —not far enough for globular cluster formation to be traced through our observations. In order to examine globular cluster formation, we must wait for third-generation gravitational-wave observatories such as the Einstein Telescope ([Punturo et al. 2010](#)) and Cosmic Explorer ([Abbott et al. 2017a](#)). These observatories, proposed to begin taking data ca. 2035, will be able to detect BBH mergers with total mass of order $O(100) M_{\odot}$ out to redshifts $z \approx 30$, and GW150914-like mergers out to $z \approx 50$ ([Hall & Evans 2019](#)).

In this paper, we demonstrate the power of gravitational-wave observations as probes of globular cluster formation and evolution. In Section 2.1, we motivate a Gaussian mixture model describing the globular cluster formation probability over cosmic time. We explain the metallicity-dependent merger time distribution used to convert this underlying globular cluster formation probability to the BBH merger probability in Section 2.2. In Section 3, we outline our population inference method. We test our ability to recover the underlying globular cluster formation probability in Section 4, obtaining population inference results using simulated third-generation gravitational-wave observatory data with realistic uncertainties. For these simulations, we use only mergers that are massive and rapid-merging—signatures of dynamical formation—as “snapshots” of the clusters at creation. We find that we can measure the formation epochs of globular clusters to 0.02–0.6 Gyr precision at 99% confidence after one year of third-generation gravitational-wave observations—comparable to the forecasted accuracy of JWST (e.g., [Correnti et al. 2016](#))—unless cluster formation primarily occurs during reionisation, in which case the precision with which we can locate a secondary lower-redshift formation epoch is reduced to $O(10)$ Gyr. If we use all cluster mergers instead of just the small fraction that we consider to be identifiable as such, our constraints on cluster forma-

¹ While Kozai-Lidov resonance ([Kozai 1962](#); [Lidov 1962](#)) is predicted to lead to eccentric mergers and mis-aligned spins, the Kozai-Lidov field merger rate is thought to be small (e.g., [Silsbee & Tremaine 2017](#); [Antonini et al. 2017](#); [Fishbach et al. 2017](#); [Rodriguez & Antonini 2018](#); [Fragione & Kocsis 2019](#)).

Parameter	Value	
	z	t [Gyr]
μ_1	2.00	3.30
σ_1	1.50	2.32
μ_2	10.00	0.48
σ_2	1.35	0.09
w_2/w_1	1/9, 1, 9	

Table 1. Parameter values chosen for our fiducial globular cluster formation probability models, used in the injection studies described in Section 4. Each of the two Gaussian peaks in our model has mean μ_j and standard deviation σ_j , where $j = 1$ refers to the SFR-driven peak and $j = 2$ refers to the reionisation-driven peak. The ratio w_2/w_1 determines the relative weight of the reionisation-driven peak against the SFR-driven peak. We vary w_2/w_1 to test our ability to recover the underlying globular cluster formation probability in three different scenarios, between which the dominant formation mechanism of clusters varies.

tion epochs tighten by up to an order of magnitude. In Section 5, we state the assumptions and caveats underlying our model. We conclude in Section 6.

2 MODEL

In the following section, we describe our model, which combines theoretically-motivated globular cluster formation probability distributions (described in Section 2.1) with simulated BBH merger distributions (described in Sections 2.2 and 2.3). We assume a flat Λ CDM Universe with $H_0 = 67.7 \text{ km s}^{-1} \text{ Mpc}^{-1}$ and $\Omega_0 = 0.307$ (Planck Collaboration et al. 2016).

2.1 Globular Cluster Formation Probability Distribution

Our globular cluster formation probability is modelled by a two-component Gaussian mixture model in redshift. The first component represents SFR-driven globular cluster formation, with mean μ_1 , standard deviation σ_1 and weight w_1 ; the other represents reionisation-driven globular cluster formation, with mean μ_2 , standard deviation σ_2 and weight w_2 .

We simulate a fiducial globular cluster formation probability using specific parameter values shown in Table 1. For the injection sets, we set the mean and standard deviation of the SFR-driven peak in order to best represent the true shape of the SFR (Madau & Dickinson 2014). The mean of the reionisation-driven peak is motivated by the results of Trenti et al. (2015); see also Ramirez-Ruiz et al. (2015).

To investigate our ability to distinguish the preferred channel of globular cluster formation, we vary the weight ratio w_2/w_1 . We consider three cases: (i) that globular clusters are formed primarily as a byproduct of the SFR, and there is a small contribution formed during reionisation ($w_2/w_1 = 1/9$); (ii) that globular clusters are formed with equal probability during reionisation and through star formation ($w_2/w_1 = 1$); and (iii) that globular clusters are formed primarily during reionisation, with a small contribution forming in accordance with the SFR ($w_2/w_1 = 9$). All three cases lead to a similar merger probability at $z = 0$, so the scenarios cannot be distinguished by existing detectors. However, third-generation detectors will be able to constrain w_2/w_1 . Our three globular cluster formation probability functions are plotted in pink in the three panels of Figure 1.

2.2 Binary Black Hole Merger Probability Distribution

In order to translate globular cluster formation probability into gravitational-wave observables, we calculate the distribution of BBH mergers in globular clusters. To simulate globular cluster evolution, we use the CMC Cluster Catalog (Kremer et al. 2020a). These simulations were computed using CMC (Joshi et al. 2000; Pattabiraman et al. 2013), a Hénon-type Monte Carlo code which includes various physical processes relevant to the dynamical formation of BH binaries including two-body relaxation, stellar and binary evolution (computed using updated versions of SSE and BSE; Hurley et al. 2000, 2002), and direct integration of small- N resonant encounters (Fregeau & Rasio 2007) including post-Newtonian effects (Rodriguez et al. 2018b). A number of parameters relevant to the long-term cluster evolution are varied within this set of simulations (namely the total cluster mass, initial virial radius, metallicity, and radial position within the Galactic potential), with values chosen to reflect the observed properties of the Milky Way globular clusters. Altogether, this catalogue nearly completely covers the full parameter space of the Milky Way globular clusters and captures the formation of a variety of astrophysical objects such as gravitational-wave sources as well as X-ray binaries, pulsars, and blue stragglers. By implementing a cluster age distribution model from El-Badry et al. (2019), Kremer et al. (2020a) estimated a BBH merger rate of roughly $20 \text{ Gpc}^{-3} \text{ yr}^{-1}$ in the local Universe, consistent with previous theoretical work on the subject (e.g., Rodriguez et al. 2016a; Askar et al. 2017; Rodriguez & Loeb 2018; Antonini & Gieles 2020) as well as with the observational rate inferred from the second LIGO/Virgo catalogue (Abbott et al. 2020c).

Each newborn globular cluster in our model has a metallicity-dependent merger time distribution. The clusters in the CMC Cluster Catalog have one of three absolute metallicities: 0.0002, 0.002, and 0.02. We combine mergers from clusters with the same metallicity, then sort the mergers into 100 time bins. We use a univariate spline to smoothly interpolate between the bin heights. We then perform a two-dimensional linear interpolation between these smoothed merger distributions of both cluster age and metallicity. To calculate the merger distribution for a cluster born at a certain redshift, we assume for simplicity that metallicity increases linearly with the age of the Universe. We assume a metallicity of $Z = 0.0002$ at a redshift of 24 and a metallicity of $Z = 0.02$ at the present day (see, e.g., Figure 6 of Lilly et al. 2002, for observationally-driven proposals for metallicity evolution over cosmic time).

We convert the sum of merger time distributions from all clusters into a probability distribution in redshift, from which we draw our source population. In Figure 1, the merger probability distributions from each of the three globular cluster formation probability models are plotted with teal curves. In Figure 2, we illustrate in grey the merger time distributions for two clusters: one formed at $z = 2$ and one formed at $z = 10$.

2.3 Rapid mergers as cluster formation snapshots

The merger time for a BBH formed dynamically in a stellar cluster is determined by three timescales: (i) the cluster formation time, (ii) the time required for BBH formation through dynamical encounters, and (iii) the gravitational-wave inspiral time from the time of last dynamical encounter to merger. The latter two timescales are sensitive to a variety of host cluster properties including total cluster mass, half-mass radius, and BH mass distribution (e.g., Rodriguez et al. 2016b; Askar et al. 2017; Kremer et al. 2020a). As a consequence, disentangling the cluster formation time distribution from

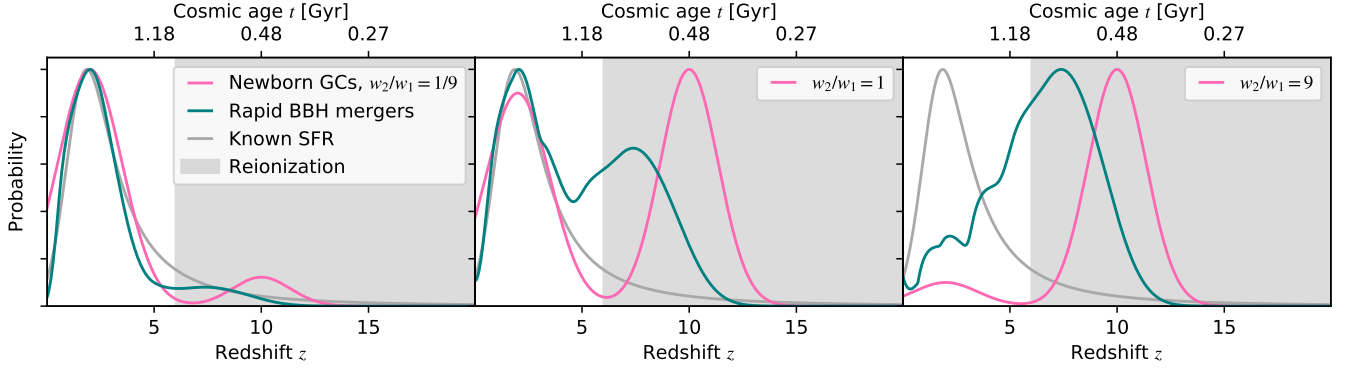


Figure 1. The three cases we consider in this work are illustrated from left to right: $w_2/w_1 = 1/9$, where SFR-driven globular cluster formation dominates clusters formed by $z = 0$; $w_2/w_1 = 1$, where there is equal contribution to clusters formed by $z = 0$ from both formation channels; and $w_2/w_1 = 9$, where reionisation-driven globular cluster formation dominates clusters formed by $z = 0$. The probability distributions of rapid-merging first-generation massive BBH mergers (where both components have $30M_\odot \leq m \leq 40M_\odot$) are plotted in teal, while the formation probability distributions of GCs in each model are plotted in pink.

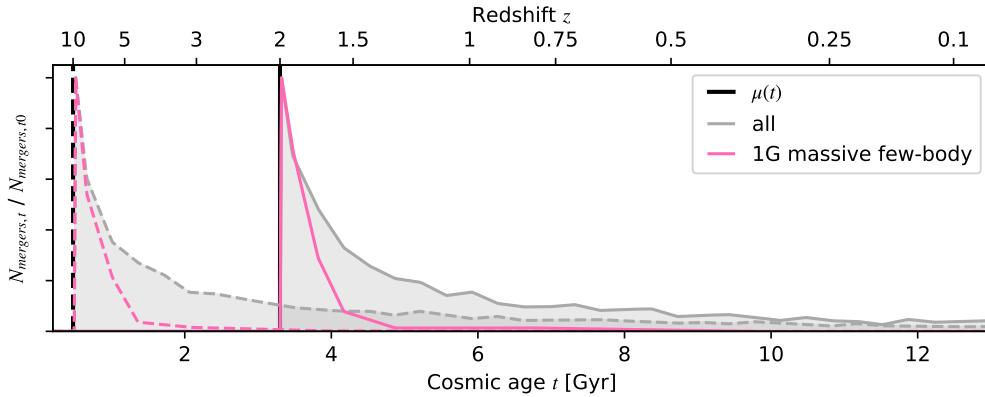


Figure 2. Merger time distributions for BBH mergers from two clusters formed at μ_1 ($z = 10$; during the peak of the SFR) and μ_2 ($z = 2$; during reionisation), with distributions shown with solid and dashed curves respectively. The distributions of all mergers from each cluster after its formation are shown in grey. The distributions of just the massive first-generation ($35M_\odot \leq m \leq 40.5M_\odot$; 1G) mergers formed through gravitational-wave capture during few-body interactions are shown in pink.

the merger time distribution for a given list of dynamical BBH mergers may pose a challenge. This challenge may be circumvented by looking at specific classes of mergers known to have prompt merger times, $t_{\text{merge}} \lesssim \mathcal{O}(100 \text{ Myr})$ since cluster formation. For these rapid mergers, the observed merger time distribution much more closely traces the underlying cluster formation time distribution.

Rapid mergers in globular clusters are expected to have two primary characteristics: high eccentricities and high masses. During small- N (‘few-body’) resonant encounters, pairs of BHs can form that merge rapidly, making them more likely to retain orbital eccentricity at detection. As discussed in [Samsing \(2018\)](#) and [Kremer et al. \(2020a\)](#), roughly 5 – 10% of cluster mergers are expected to retain high eccentricity ($e \geq 0.1$) close to merger ($f_{\text{GW}} = 10 \text{ Hz}$). These binaries can have gravitational-wave inspiral times as short as days (e.g., [Zevin et al. 2019](#)); this makes them ideal tracers of cluster formation, as they merge relatively quickly after the cluster forms and are more likely to retain the dynamically-induced eccentricity that can reveal their formation channel. As a natural consequence of dynamical friction, the most massive BHs in a cluster are expected, on average, to be the first to form BBHs and the first to merge (e.g., [Morscher et al. 2015](#)). Thus, BHs with masses near the assumed up-

per limit of the BH mass distribution ($40.5M_\odot$ in the CMC Cluster Catalog) that merge through gravitational-wave capture encounters are ideal rapid merger candidates. For the analysis presented in Section 4, we consider only globular cluster binaries that merge through resonant few-body encounters.

There is an inherent additional delay associated with second-generation BHs formed through previous BH mergers that remain bound to their host cluster. Although these will preferentially merge again quickly (within a few 10 Myr of the previous merger) due to their relatively high mass, we do not include second-generation mergers in this analysis. Here, we consider only those massive few-body mergers that are first-generation (1G), having both component masses above $35M_\odot$ and below $40.5M_\odot$. We plot this distribution of mergers in pink in Figure 2. Over the redshift range that we study, the fraction of 1G massive few-body mergers varies between 3% and 6% of all cluster mergers. We construct the merger time distribution using only 1G massive few-body mergers, and draw only 5% of the number of detections expected from the observing durations.

3 METHOD

We simulate redshift posterior probability distributions for a population of BBH mergers, and use the population inference framework to discern the injected distribution of the population. The likelihood for the data \mathbf{d} is

$$\mathcal{L}_{tot}(\mathbf{d}|\Lambda) = \prod_i \frac{\mathcal{Z}_\emptyset(d_i)}{n_i} \sum_k \frac{\pi(\theta_i^k|\Lambda)}{\pi(\theta_i^k|\emptyset)}. \quad (1)$$

In this equation, Λ is the set of parameters describing the population distribution, while θ_i^k are the parameters describing the k th posterior sample of event i (in our case, θ_i is only one parameter – redshift). Each event i has n_i posterior samples; there are a total of N events. The sampling prior used for inference on data d_i for event i is $\pi(\theta_i|\emptyset)$, which is reweighted to obtain results for a population-based prior $\pi(\theta_i|\Lambda)$. The evidence obtained with the original sampling is $\mathcal{Z}_\emptyset(d_i)$. In our case, the population prior $\pi(\theta_i|\Lambda)$ is the distribution described in Section 2.

Distance measurement uncertainties are likely to be $O(10\%)$ for most binaries observed with third-generation detectors (Vitale & Evans 2017; Zhao & Wen 2018). To model uncertainty of approximately this magnitude, we assume Gaussian likelihoods of width $\sigma_{z_i} = 0.1z_i$. These likelihoods each have a mean $\mu_{z_i} = z_i + r_i$, where r_i is a random offset drawn from a Gaussian of mean $\mu_{r_i} = 0$ and $\sigma_{r_i} = \sigma_{z_i}$. We produce a posterior curve by multiplying the likelihood by a uniform sampling prior. (This prior is divided out in the calculation of Eq. 1.) From this posterior curve, we draw 50 simulated posterior samples for each event.

To execute our population analysis, we use the Bayesian inference library bilby (Ashton et al. 2019; Romero-Shaw et al. 2020a). We use uniform priors over all parameters. The prior covers the range $10^{-5} \leq z \leq 6$ for μ_1 , $0.5 \leq z \leq 6$ for both σ values, and $6 \leq z \leq 20$ for μ_2 . The prior on w_2/w_1 ranges from 10^{-2} to 10.

The formation channel of a binary may be identified using a method such as that developed in Kimball et al. (2020a), in which a BBH merger’s mass and spin measurements are used to calculate its probability of being a hierarchical merger in a globular cluster. Similar methods may be extended to incorporate eccentricity measurements, which will be illuminating for globular clusters as we expect $\sim 5\%$ of globular cluster mergers to have eccentricity $e \geq 0.1$ at 10 Hz (see, e.g., Samsing 2018). While precession is considered a hallmark of dynamical mergers, there have been relatively few events that have clear precession measurements (Abbott et al. 2019; Abbott et al. 2020c); however, both precession and anti-aligned spins can be measured at a population level, as demonstrated in (Abbott et al. 2020d). With third-generation detectors, component spins and precession will be well measured (e.g., Vitale & Whittle 2018). Using such measurements at both an individual and population level, it may be possible to estimate the sub-population of globular cluster mergers within a set of BBH mergers from a variety of formation channels.

In this paper, we assume that mergers identified as cluster mergers have 0% probability of having formed via a different channel. Such definitive statements are unlikely to be made based on the parameters of detected binaries for the vast majority of sources even if we allow for future improvements to our mechanisms for performing such identifications. In the future, binaries that form in globular clusters but are kicked out before merging may still be indistinguishable from isolated mergers, and those that do merge inside the cluster are likely to have properties similar to those in other dynamical environments (e.g., AGN discs and galactic nuclei) or field triples undergoing Kozai-Lidov resonance. More complex future analyses should weight the samples from each event by the probability that

μ_1	99% CI width (Gyr)		
w_2/w_1	Day	Month	Year
9	11.92	12.01	10.49
1	11.99	9.87	0.53
1/9	10.44	4.32	0.39
μ_2			
9	0.48	0.06	0.02
1	0.74	0.08	0.02
1/9	0.74	0.42	0.05

Table 2. Width of 99% credible intervals (CIs) around μ_1 (top) and μ_2 (bottom) for each injection study described in Section 4. For these injection studies we use only first-generation massive few-body mergers, and include a 10% uncertainty on source redshift. When the 10% uncertainty is removed, the width of these uncertainty intervals does not meaningfully change.

each binary formed inside a globular cluster. This is an additional complication that can be built upon the method presented here, and is left for future work.

4 INJECTION STUDIES

The Universal merger rate implied by current BBH merger observations is $\sim 0.2 \text{ min}^{-1}$ (Abbott et al. 2018). For an all-seeing detector, this translates to a BBH signal detection count of $O(500)$ per day (Maggiore et al. 2020). Third-generation detectors like CE and ET will be close to all-seeing, detecting GW150914-like events out to redshifts $z \approx 50$, and GW190521-like out to $z \approx 30$ (Hall & Evans 2019). We use 500, 10000 and 100000 as order-of-magnitude estimates for the total number of GC mergers in one day, one month and one year, respectively. This is a reasonable approximation if GC mergers make up $\geq 10\%$ of all mergers in the Universe. We assume, based on the fraction of massive and quick-merging binaries observed in the cluster simulations described in Section 2, that only 5% of these observations can be confidently identified as cluster mergers. To simulate a month’s worth of confidently-identified cluster mergers, for example, we use 500 events.

We simulate data after one day, one month, and one year of observing, for three different models of the underlying globular cluster formation probability. The first case we consider is one where globular clusters do not form efficiently during reionisation. In this case, the globular cluster formation probability curve closely follows the observed SFR. We set the weight ratio $w_2/w_1 = 1/9$, such that 90% of all clusters form within the SFR peak. In the second case, we set the weight ratio $w_2/w_1 = 1$, which leads to a 50–50 split between clusters contributed from each peak. The final case we consider is one where globular clusters primarily form during reionisation, such that 90% of clusters are formed within the reionisation peak. We set $w_2/w_1 = 9$. For all three injected data sets, the remaining four parameters ($\mu_1, \mu_2, \sigma_1, \sigma_2$) are fixed to the values provided in Table 1. We show the globular cluster formation probability curve and resulting probability distribution of observable BBH mergers for all three cases in Figure 1.

In Figure 3, we plot the injected underlying globular cluster formation probability curve in pink, and compare it to the recovered median and 99% confidence intervals in grey. For all three observing periods, the injected distribution is within the 99% confidence interval. Probability distributions on the five populations parameters $\mu_1, \mu_2, \sigma_1, \sigma_2$ and w_2/w_1 are provided as corner plots in Appendix A.

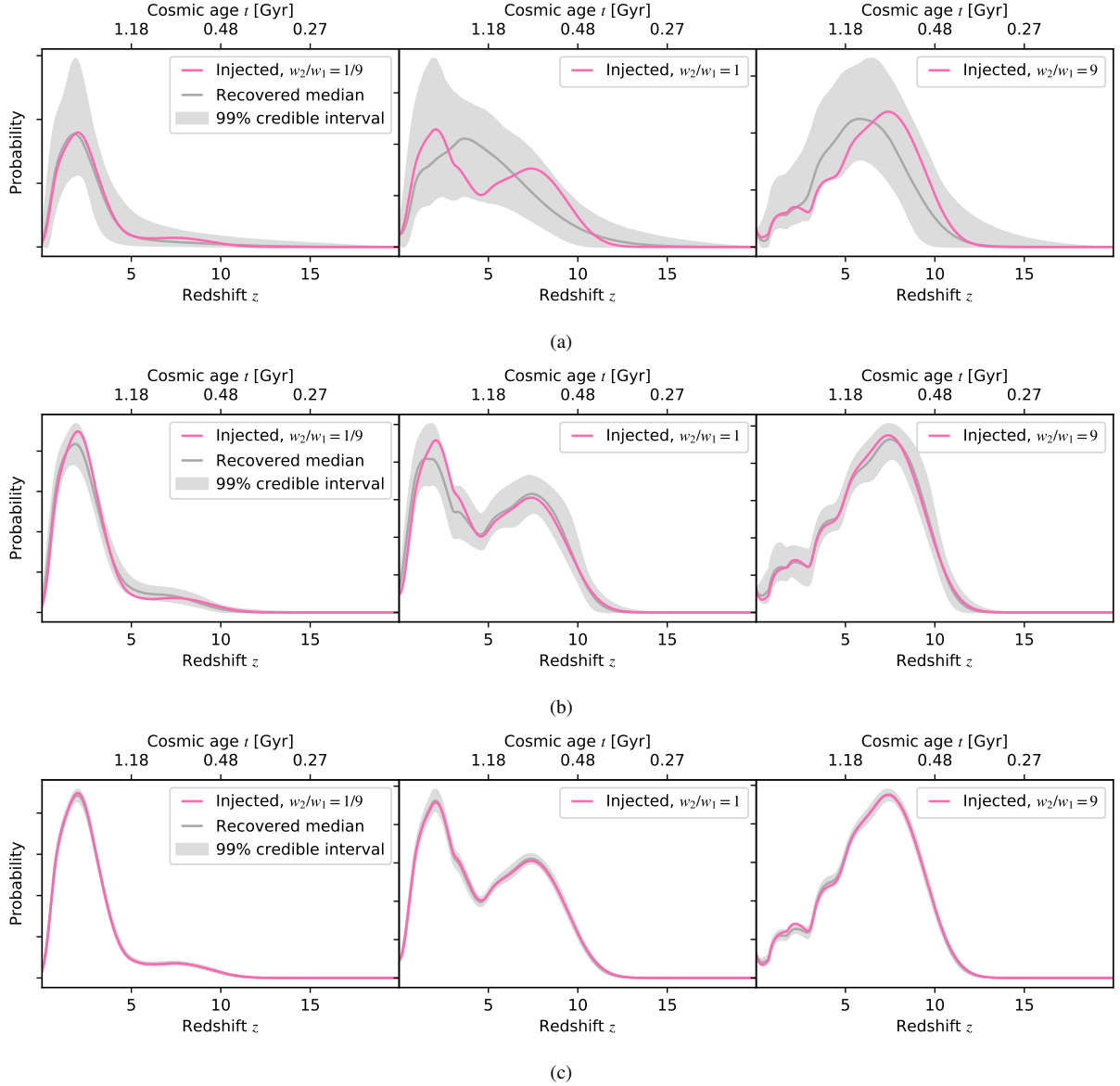


Figure 3. Globular cluster formation rates inferred from simulated third-generation detector observations of first-generation massive few-body mergers after (a) one day (using 25 1G massive few-body mergers from the total population of 500), (b) one month (using 500 of 10000) and (c) one year of detections (using 5000 of 100000). Each panel represents an underlying model with a different weighting of the two components of the Gaussian mixture model that represents the globular cluster formation rate. *Left:* SFR-driven peak dominates formation rate; *Middle:* Each peak contributes equally to formation rate; *Right:* Reionisation-driven peak dominates formation rate.

We state the widths of the 99% confidence intervals around μ_1 and μ_2 for each study in Table 2.

We repeat the above injection studies for two additional scenarios. In the first, we neglect any measurement uncertainty and assume that each source is represented by a delta function at its true value of z . In this case, we see negligible change in the widths of the 99% credible intervals around μ_1 and μ_2 . In the second, we include redshift measurement uncertainty, but optimistically assume that all cluster mergers can be confidently identified, thereby allowing us to use 100% of the mergers from the CMC Cluster Catalog to construct our model. This leads to a reduction of up to an order of magnitude in the width of the 99% credible interval around μ_1 and μ_2 ; for one day of observing all cluster mergers, the credible intervals are nearly identical to those seen for a month of observing only 1G massive

few-body mergers. These measurements are more precise—despite the longer average merger timescale—because we are able to use 20 times as many events to probe the cluster formation rate. The precision with which we can measure globular cluster formation epochs with third-generation observations, therefore, sensitively depends on the number of events that are confidently identified as globular cluster mergers.

5 SYSTEMATIC ERROR ANALYSIS AND CAVEATS

We make a number of simplifying assumptions and approximations in our analysis, allowing us to demonstrate a generic way to probe globular cluster formation using gravitational-wave detections. These

are listed in this section, with the aim to reduce the number of assumptions we make in future work that builds upon this paper.

We approximate both epochs of globular cluster formation as simple Gaussians in redshift. However, the true SFR determining the shape of the cluster formation probability does not follow a Gaussian, and the shape of the reionisation-driven cluster formation probability is not known. More complex future extensions of this work may allow the shape of the Gaussians to vary, with the skewness of the Gaussian a model variable. We assume that the redshift posterior distributions are also Gaussian, but the true shape of the uncertainty distribution would vary depending on the noise in the data containing each signal.

We set our injection studies in an optimistic future where merger channels can be perfectly distinguished. While we analyse the merger distribution of only those globular cluster BBH that are high-mass, rapid-merging and highly likely to be detectably eccentric (signatures of dynamical origin) for our primary results, we still ignore any possibility of contamination from other dynamical formation channels that produce mergers with similar properties, such as mergers in AGN or Kozai-Lidov (Kozai 1962; Lidov 1962) triples in the field.

We also do not account for any sources redshifting out-of-band due to high masses or high eccentricities at high redshift. We do not account for the disruption/creation of globular clusters during galaxy mergers; while the increased star formation of merging galaxies should be absorbed into the SFR peak of our models, the shape of the merger time distribution at a given epoch will differ if clusters are disrupted/created at that time due to galaxy mergers, even if the overall number of globular clusters remains the same.

We assume that metallicity increases linearly with the age of the Universe to obtain different merger time distributions for clusters born at different times, but do not consider a time-evolving initial mass/density function. Metallicity, mass and density may become globular cluster variables in future iterations of our model, allowing us to consider whether the physical properties of clusters can be inferred from observations of gravitational waves.

6 CONCLUSIONS

In this work, we show that observations from third-generation gravitational-wave detectors will allow us to measure the formation epochs of the population of globular clusters. Our primary results are obtained assuming that only first-generation massive few-body mergers can be confidently identified as globular cluster mergers. If up to 50% of clusters are born following the SFR, a cluster formation epoch at $z = 2$ can be resolved to within less than 1 Gyr precision after one year of observing; however, if the majority of clusters are born during reionisation, the time of this epoch will have an uncertainty $O(10)$ Gyr. For all scenarios, a cluster formation epoch at $z = 10$ can be resolved to within less than 1 Gyr precision after just one day of observing, and to within 0.05 Gyr after a full year. If we are able to confidently identify all globular cluster mergers as such, these uncertainty bands can decrease by up to an order of magnitude. With third-generation detectors Cosmic Explorer and Einstein Telescope due to commence observing in the 2030s (Reitze et al. 2019; Maggione et al. 2020), the question of how globular clusters formed may be answered with gravitational-wave observations within the next twenty years. These results will be complementary to measurements from electromagnetic telescopes, such as JWST, which will be able to constrain the ages of individual clusters to within $O(1)$ Gyr (e.g., Correnti et al. 2016).

Our method can be extended for use in multiple future projects. For

example, we could assign a population of mergers from multiple formation channels with a certain probability of being globular cluster mergers, and weight their contribution to the total merger distribution accordingly. We could also use intrinsic binary parameters, e.g. mass and eccentricity, to infer properties of their host clusters, like their densities at formation. The simple procedure outlined in this paper must be refined before application to real data. In particular, future work should address the fact that many signals from the more massive and highly-eccentric sources may be redshifted out-of-band. We leave potential extensions and improvements for future work.

DATA AVAILABILITY

We use publicly available output from the globular cluster simulations of Kremer et al. (2020a), and perform our analysis using publicly available Bayesian inference library bilby (Ashton et al. 2019; Romero-Shaw et al. 2020a).

ACKNOWLEDGEMENTS

We thank Duncan Forbes and Michele Trenti for sharing with us their expertise in globular cluster formation scenarios. We also thank Michela Mapelli and Christopher Berry for their comments, which improved the manuscript, and our anonymous reviewer, whose suggestions improved both the paper and the science it contains. KK is supported by an NSF Astronomy and Astrophysics Postdoctoral Fellowship under award AST-2001751. PDL and ET are supported through Australian Research Council Future Fellowships FT160100112 and FT150100281, ARC Discovery Project DP180103155, and ARC Centre of Excellence CE170100004. JS is supported by the European Unions Horizon 2020 research and innovation programme under the Marie Skłodowska-Curie grant agreement No. 844629.

REFERENCES

- Aasi J., et al., 2015, *cqg*, **32**, 074001
- Abbott B. P., Abbott R., Abbott T. D., et al., 2016, *prx*, **6**, 041015
- Abbott B. P., et al., 2017a, *Class. Quant. Grav.*, **34**, 044001
- Abbott B. P., Abbott R., Abbott T. D., et al., 2017b, *pri*, **119**, 161101
- Abbott B. P., Abbott R., Abbott T. D., et al., 2017c, *ApJ*, **848**, L12
- Abbott B. P., Abbott R., Abbott T. D., Acernese F., et al., 2018, *pri*, **120**, 091101
- Abbott B. P., et al., 2019, *Phys. Rev. X*, **9**, 031040
- Abbott R., Abbott T. D., Abraham S., Acernese F., Ackley K., et al., 2020a, *Astrophys. J.*
- Abbott R., Abbott T. D., Abraham S., Acernese F., et al., 2020b, arXiv e-prints, [p. arXiv:2009.01075](https://arxiv.org/abs/2009.01075)
- Abbott R., Abbott T. D., Abraham S., Acernese F., Ackley K., Adams A., Adams C., et al., 2020c, arXiv e-prints, [p. arXiv:2010.14527](https://arxiv.org/abs/2010.14527)
- Abbott R., Abbott T. D., Abraham S., Acernese F., Ackley K., Adams A., Adams C., et al., 2020d, arXiv e-prints, [p. arXiv:2010.14533](https://arxiv.org/abs/2010.14533)
- Acernese F., et al., 2015, *Classical Quantum Gravity*, **32**, 024001
- Antonini F., Giesels M., 2020, arXiv e-prints, [p. arXiv:2009.01861](https://arxiv.org/abs/2009.01861)
- Antonini F., Toonen S., Hamers A. S., 2017, *Astrophys. J.*, **841**, 77
- Ashton G., et al., 2019, *Astrophys. J. Suppl.*, **241**, 27
- Askar A., Szkudlarek M., Gondek-Rosińska D., Giersz M., Bulik T., 2017, *MNRAS*, **464**, L36
- Bavera S. S., et al., 2021, *A&A*, **647**, A153
- Belczynski K., 2020, arXiv e-prints, [p. arXiv:2009.13526](https://arxiv.org/abs/2009.13526)
- Bethe H. A., Brown G. E., 1998, *Astrophys. J.*, **506**, 780
- Campanelli M., Lousto C. O., Zlochower Y., 2006, *Phys. Rev. D*, **D74**, 084023

- Correnti M., Gennaro M., Kalirai J. S., Brown T. M., Calamida A., 2016, *ApJ*, **823**, 18
- Di Carlo U. N., Giacobbo N., Mapelli M., Pasquato M., Spera M., Wang L., Haardt F., 2019, *MNRAS*, **487**, 2947
- El-Badry K., Quataert E., Weisz D. R., Choksi N., Boylan-Kolchin M., 2019, *MNRAS*, **482**, 4528
- Elmegreen B. G., 2010, *The Astrophysical Journal*, **712**, L184
- Elmegreen D. M., Elmegreen B. G., 2017, *ApJ*, **851**, L44
- Fall S. M., Rees M. J., 1985, *ApJ*, **298**, 18
- Fishbach M., Holz D. E., 2017, *Astrophys. J.*, **851**, L25
- Fishbach M., Holz D. E., Farr B., 2017, *Astrophys. J.*, **840**, L24
- Forbes D. A., Bridges T., 2010, *MNRAS*, **404**, 1203
- Forbes D. A., Pastorello N., Romanowsky A. J., Usher C., Brodie J. P., Strader J., 2015, *MNRAS*, **452**, 1045
- Forbes D. A., et al., 2018, *Proceedings of the Royal Society of London Series A*, **474**, 20170616
- Fragione G., Kocsis B., 2018, *Phys. Rev. Lett.*, **121**
- Fragione G., Kocsis B., 2019, arXiv e-prints, p. arXiv:1910.00407
- Fregeau J. M., Rasio F. A., 2007, *apj*, **658**, 1047
- García-Berro E., Torres S., Althaus L. r. G., Miller Bertolami M. M., 2014, *A&A*, **571**, A56
- Gerosa D., Berti E., 2017, *Phys. Rev.*, **D95**, 124046
- Gondán L., Kocsis B., 2019, *Astrophys. J.*, **871**, 178
- Gratton R. G., Fusi Pecci F., Carretta E., Clementini G., Corsi C. E., Lattanzi M., 1997, *ApJ*, **491**, 749
- Gröbner M., Ishibashi W., Tiwari S., Haney M., Jetzer P., 2020, *A&A*, **638**, A119
- Hall E. D., Evans M., 2019, *Classical and Quantum Gravity*, **36**, 225002
- Hansen B. M. S., et al., 2013, *Nature*, **500**, 51
- Heger A., Woosley S. E., 2002, *Astrophys. J.*, **567**, 532
- Hinder I., Vaishnav B., Herrmann F., Shoemaker D., Laguna P., 2008, *Phys. Rev. D*, **D77**, 081502
- Hoang B.-M., Naoz S., Kocsis B., Rasio F. A., Dosopoulou F., 2018, *ApJ*, **856**, 140
- Hong J., Vesperini E., Askar A., Giersz M., Szkudlarek M., Bulik T., 2018, *MNRAS*, **480**, 5645
- Hurley J. R., Pols O. R., Tout C. A., 2000, *MNRAS*, **315**, 543
- Hurley J. R., Tout C. A., Pols O. R., 2002, *MNRAS*, **329**, 897
- Ivanova N., et al., 2013, *A&ARv*, **21**, 59
- Joshi K. J., Rasio F. A., Zwart S. P., Portegies Zwart S., 2000, *The Astrophysical Journal*, **540**, 969
- Kalogera V., 2000, *ApJ*, **541**, 319
- Katz H., Ricotti M., 2014, *Monthly Notices of the Royal Astronomical Society*, **444**, 2377
- Kerber L. O., et al., 2019, *MNRAS*, **484**, 5530
- Kimball C., Talbot C., Berry C. P. L., Carney M., Thrane E., Kalogera V., 2020a, arXiv e-prints, p. arXiv:2005.00023
- Kimball C., et al., 2020b, arXiv e-prints, p. arXiv:2011.05332
- Kimm T., Cen R., Rosdahl J., Yi S. K., 2016, *ApJ*, **823**, 52
- Kozai Y., 1962, *Astrophys. J.*, **67**, 591
- Kremer K., et al., 2020a, *ApJS*, **247**, 48
- Kremer K., et al., 2020b, *ApJ*, **903**, 45
- Kruckow M. U., Tauris T. M., Langer N., Szécsi D., Marchant P., Podsiadlowski P., 2016, *Astron. Astrophys.*, **596**, A58
- Kruijssen J. M. D., 2015, *Monthly Notices of the Royal Astronomical Society*, **454**, 1658
- Lada C. J., Lada E. A., 2003, *ARA&A*, **41**, 57
- Leaman R., VandenBerg D. A., Mendel J. T., 2013, *MNRAS*, **436**, 122
- Lidov M. L., 1962, *Planetary and Space Science*, **9**, 719
- Lilly S. J., Carollo C. M., Stockton A. N., 2002, arXiv e-prints, pp astro-ph/0209243
- Livio M., Soker N., 1988, *Astrophys. J.*, **329**, 764
- Ma X., Quataert E., Wetzell A., Faucher-Giguère C.-A., Boylan-Kolchin M., 2020, arXiv e-prints, p. arXiv:2006.10065
- Madau P., Dickinson M., 2014, *ARA&A*, **52**, 415
- Maggiore M., et al., 2020, *J. Cosmology Astropart. Phys.*, **2020**, 050
- Majewski S. R., Patterson R. J., Dinescu D. I., Johnson W. Y., Osthheimer J. C., Kunkel W. E., Palma C., 2000, in Noels A., Magain P., Caro D., Jehin E., Parmentier G., Thoul A. A., eds, *Liege International Astrophysical Colloquia Vol. 35, Liege International Astrophysical Colloquia*. p. 619 (arXiv:astro-ph/9910278)
- Morscher M., Pattabiraman B., Rodriguez C., Rasio F. A., Umbreit S., 2015, *ApJ*, **800**, 9
- NASA 2020, NASA Announces New James Webb Space Telescope Target Launch Date, *NASA press release*, www.nasa.gov/press-release/nasa-announces-new-james-webb-space-telescope-target-launch-date
- Neijssel C. J., et al., 2019, *MNRAS*, **490**, 3740
- Pattabiraman B., Umbreit S., Liao W.-k., Choudhary A., Kalogera V., Memik G., Rasio F. A., 2013, *The Astrophysical Journal Supplement Series*, **204**, 15
- Peacock M. B., Maccarone T. J., Knigge C., Kundu A., Waters C. Z., Zepf S. E., Zurek D. R., 2010, *Mon. Not. Roy. Astron. Soc.*, **402**, 803
- Peters P. C., 1964, *Phys. Rev.*, **136**, B1224
- Planck Collaboration Ade P. A. R., Aghanim N., Arnaud M., Ashdown M., Aumont J., Baccigalupi C., et al., 2016, *A&A*, **594**, A13
- Punturo M., et al., 2010, *Class. Quant. Grav.*, **27**, 194002
- Ramirez-Ruiz E., Trenti M., MacLeod M., Roberts L. F., Lee W. H., Saladino-Rosas M. I., 2015, *ApJ*, **802**, L22
- Reitze D., et al., 2019, in Bulletin of the American Astronomical Society. p. 35 (arXiv:1907.04833)
- Rodriguez C. L., Antonini F., 2018, *Astrophys. J.*, **863**, 7
- Rodriguez C. L., Loeb A., 2018, preprint, (arXiv:1809.01152)
- Rodriguez C. L., Morscher M., Pattabiraman B., Chatterjee S., Haster C.-J., Rasio F. A., 2015, *Physical review letters*, **115**, 051101
- Rodriguez C. L., Chatterjee S., Rasio F. A., 2016a, *Physical Review D*, **93**, 084029
- Rodriguez C. L., Zevin M., Pankow C., Kalogera V., Rasio F. A., 2016b, *Astrophys. J.*, **832**, L2
- Rodriguez C. L., Amaro-Seoane P., Chatterjee S., Rasio F. A., 2018a, *Phys. Rev. Lett.*, **120**, 151101
- Rodriguez C. L., Amaro-Seoane P., Chatterjee S., Rasio F. A., 2018b, *Physical Review Letters*, **120**, 151101
- Rodriguez C. L., Amaro-Seoane P., Chatterjee S., Kremer K., Rasio F. A., Samsing J., Ye C. S., Zevin M., 2018c, *Phys. Rev.*, **D98**, 123005
- Romero-Shaw I. M., et al., 2020a, *mnras*, **499**, 3295
- Romero-Shaw I., Lasky P. D., Thrane E., Calderón Bustillo J., 2020b, *ApJ*, **903**, L5
- SEDS Messier Database 2020, Milky Way Globular Clusters, https://www.messier.seds.org/xtra/supp/mw_gc.html
- Safarzadeh M., Berger E., Ng K. K. Y., Chen H.-Y., Vitale S., Whittle C., Scannapieco E., 2019, *ApJ*, **878**, L13
- Samsing J., 2018, *Phys. Rev. D*, **D97**, 103014
- Samsing J., D’Orazio D. J., 2018, *Mon. Not. Roy. Astron. Soc.*, **481**
- Samsing J., Hotokezaka K., 2020, arXiv e-prints, p. arXiv:2006.09744
- Samsing J., MacLeod M., Ramirez-Ruiz E., 2014, *ApJ*, **784**, 71
- Samsing J., D’Orazio D. J., Askar A., Giersz M., 2018, arXiv e-prints, p. arXiv:1802.08654
- Sarajedini A., et al., 2007, *AJ*, **133**, 1658
- Shapiro K. L., Genzel R., Förster Schreiber N. M., 2010, *Monthly Notices of the Royal Astronomical Society: Letters*, **403**, L36
- Silsbee K., Tremaine S., 2017, *Astrophys. J.*, **836**, 39
- Stevenson S., Berry C. P. L., Mandel I., 2017, *Mon. Not. Roy. Astron. Soc.*, **471**, 2801
- Tagawa H., Kocsis B., Saitoh T. R., 2018, *Phys. Rev. Lett.*, **120**, 261101
- Talbot C., Thrane E., 2017, *Phys. Rev. D*, **96**, 023012
- Talbot C., Thrane E., 2018, *Astrophys. J.*, **856**, 173
- Tamura N., Sharples R. M., Arimoto N., Onodera M., Ohta K., Yamada Y., 2006, *MNRAS*, **373**, 588
- Trenti M., Padoan P., Jimenez R., 2015, *ApJ*, **808**, L35
- VandenBerg D. A., Brogaard K., Leaman R., Casagrande L., 2013, *ApJ*, **775**, 134
- Vitale S., Evans M., 2017, *Phys. Rev. D*, **95**, 064052
- Vitale S., Whittle C., 2018, *Phys. Rev. D*, **98**, 024029
- Vitale S., Farr W. M., Ng K. K. Y., Rodriguez C. L., 2019, *ApJ*, **886**, L1
- Wang L., et al., 2016, *MNRAS*, **458**, 1450

- Zevin M., Samsing J., Rodriguez C., Haster C.-J., Ramirez-Ruiz E., 2019, [Astrophys. J.](#), 871, 91
- Zevin M., et al., 2020, arXiv e-prints, p. [arXiv:2011.10057](#)
- Zhao W., Wen L., 2018, [Phys. Rev. D](#), 97, 064031
- de Mink S. E., Mandel I., 2016, [Mon. Not. Roy. Astron. Soc.](#), 460, 3545
- de Mink S. E., Cantiello M., Langer N., Pols O. R., 2010, in Kalogera V., van der Sluys M., eds, American Institute of Physics Conference Series Vol. 1314, American Institute of Physics Conference Series. pp 291–296 ([arXiv:1010.2177](#)), [doi:10.1063/1.3536387](#)
- van den Heuvel E. P. J., Portegies Zwart S. F., de Mink S. E., 2017, [MNRAS](#), 471, 4256

APPENDIX A: POSTERIOR PROBABILITY DISTRIBUTIONS FOR POPULATION PARAMETERS

In this section, we present posterior probability distributions for our five population parameters in cosmic time, recovered using the merger-time distributions of 1G massive few-body mergers. Posterior distributions are plotted in grey, with the injected values indicated with pink lines, and the shading gradients on the two-dimensional posteriors indicate levels of 1σ , 2σ and 3σ credibility, while the dashed grey error bars around the median recovered values show 99% confidence intervals.

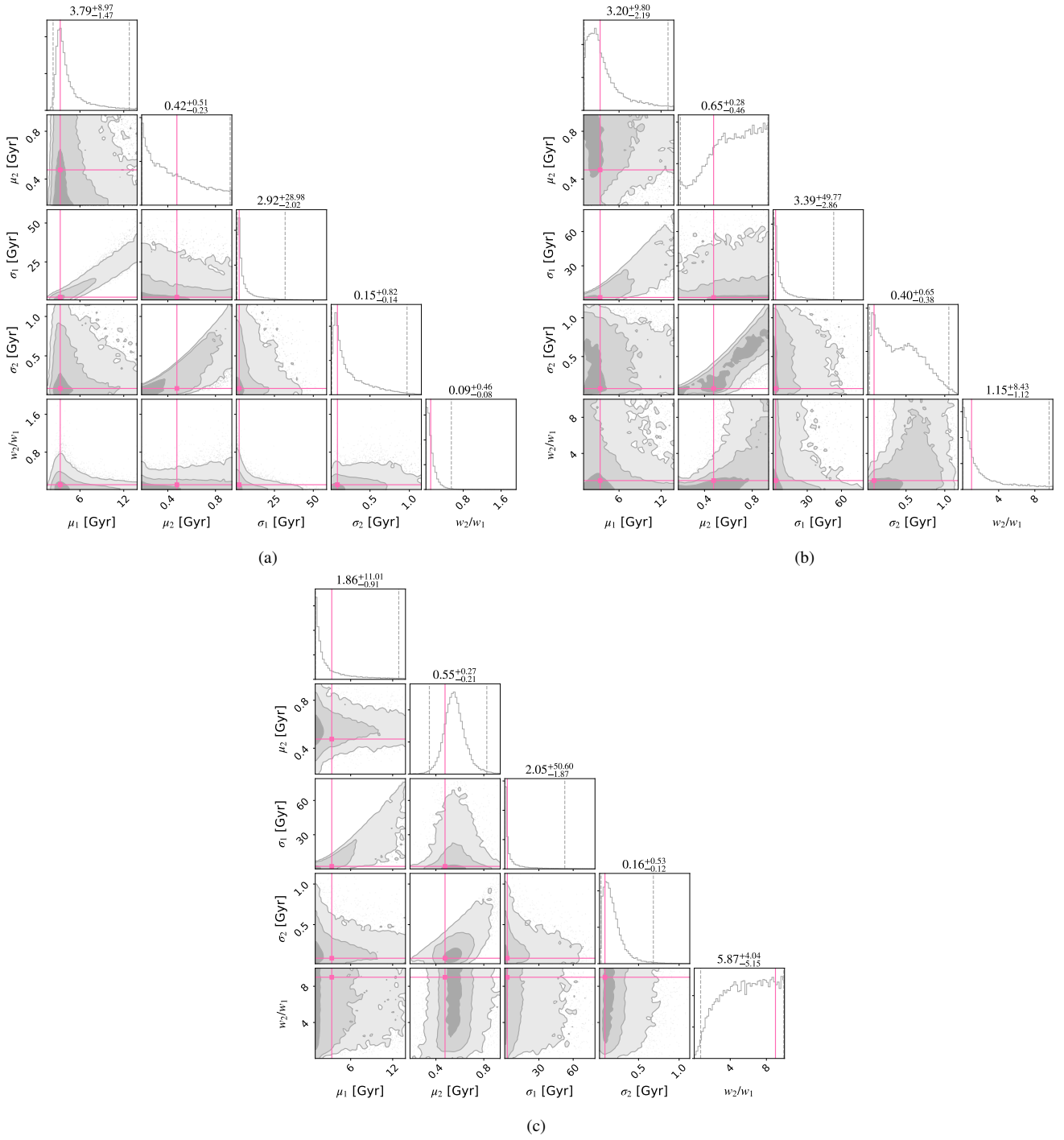


Figure A1. Posterior probability distributions on our five population parameters after one day of simulated third-generation detector observations of massive few-body mergers from globular clusters (25 events). Results are shown for three variations on our two-component Gaussian mixture model: (a) $w_2/w_1 = 1/9$, (b) $w_2/w_1 = 1$, and (c) $w_2/w_1 = 9$.

A1 Results after one day of observing

In Figure A1 we present the one- and two-dimensional posterior probability distributions over each population parameter resolved after one day of observations with third-generation detectors.

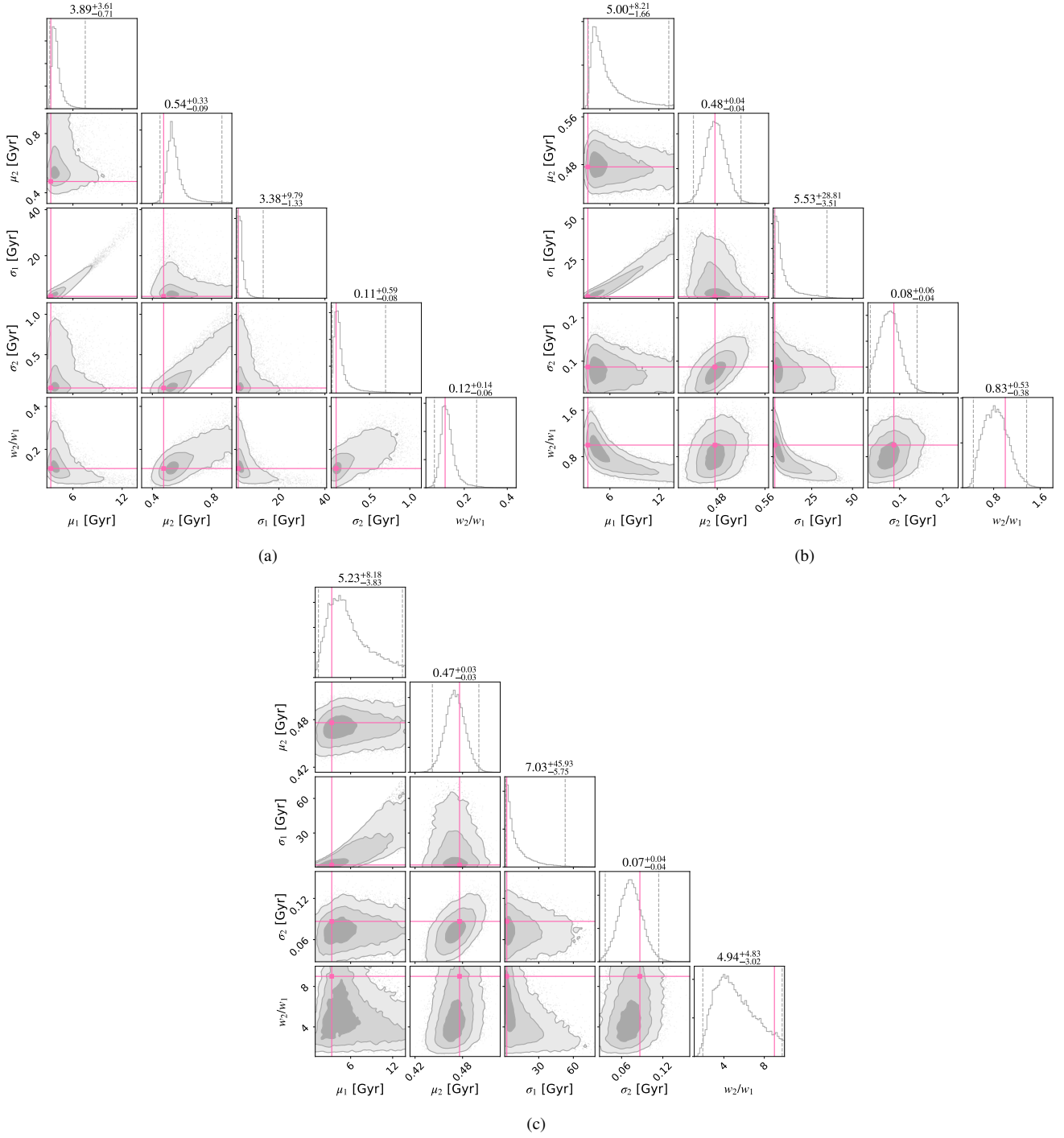


Figure A2. Posterior probability distributions on our five population parameters after one month of simulated third-generation detector observations of massive few-body mergers from globular clusters (500 events). Results are shown for three variations on our two-component Gaussian mixture model: (a) $w_2/w_1 = 1/9$, (b) $w_2/w_1 = 1$, and (c) $w_2/w_1 = 9$.

A2 Results after one month of observing

In Figure A2 we present the one- and two-dimensional posterior probability distributions over each population parameter resolved after one day of observations with third-generation detectors.

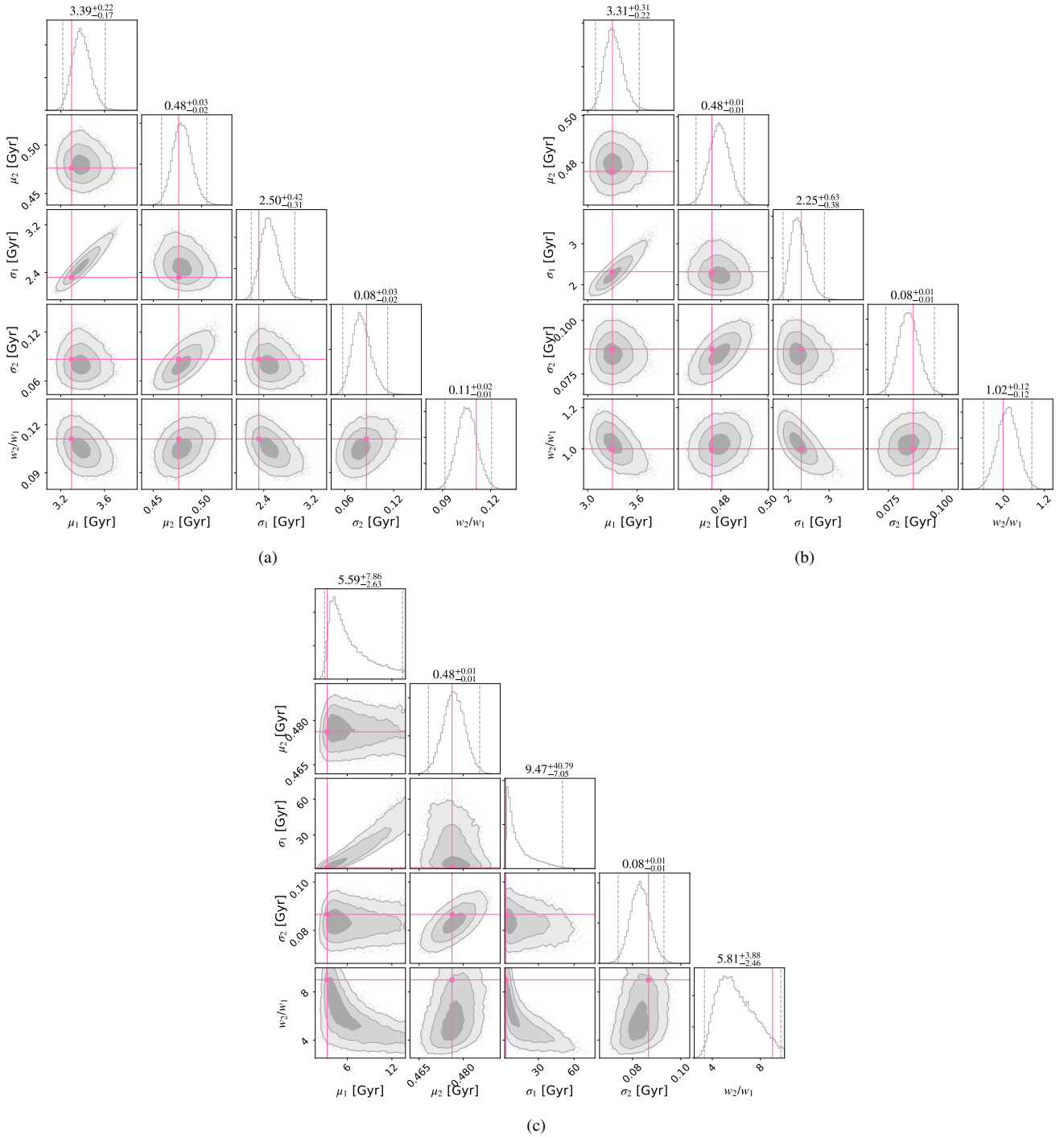


Figure A3. Posterior probability distributions on our five population parameters after one year of simulated third-generation detector observations of massive few-body mergers from globular clusters (5000 events). Results are shown for three variations on our two-component Gaussian mixture model: (a) $w_2/w_1 = 1/9$, (b) $w_2/w_1 = 1$, and (c) $w_2/w_1 = 9$.

A3 Results after one year of observing

In Figure A3 we present the one- and two-dimensional posterior probability distributions over each population parameter resolved after one day of observations with third-generation detectors.

This paper has been typeset from a \LaTeX file prepared by the author.